Geochemical evolution of tourmaline in the Darasun gold district, Transbaikal region, Russia: Evidence from chemical and boron isotopic compositions

Ivan A. Baksheev, Vsevolod Yu. Prokofiev, Robert B. Trumbull, Michael Wiedenbeck, Vasilii O. Yapaskurt

I. A. Baksheev (corresponding author), V. O. Yapaskurt

Geology Department, Moscow State University, Leninskie Gory, Moscow 119234, Russia

e-mail: ivan.baksheev@gmail.com, Phone: +7-495-9394676, Fax: +7-495-9328889

V. Yu. Prokofiev

Institute of Geology of Ore Deposits, Petrography, Mineralogy, and Geochemistry, Russian Academy of Sciences, Moscow 119017, Russia

Geology Department, Moscow State University, Leninskie Gory, Moscow 119234, Russia

R. B. Trumbull, M. Wiedenbeck

GFZ German Research Centre for Geosciences, Telegrafenberg 14473 Potsdam, Germany

Abstract The Darasun gold district, Transbaikal region, eastern Russia comprises three deposits: Teremkyn, Talatui, and Darasun, where gold-bearing quartz veins are hosted in metagabbro and granitoids. Tourmaline is a common gangue mineral in these deposits and a useful indicator of fluid source. The tourmaline compositions are oxy-dravite--povondraite, dravite, and schorl. We report here in-situ B-isotope analyses by SIMS on tourmaline from veins in metagabbro and K-rich granodiorite, as well as from a breccia pipe at the margin of granodiorite porphyry. The B-isotope composition of tourmalines from the Darasun gold district as a whole covers a very wide range from -15.7 to +11.2‰, with distinctive differences among the three deposits. The $\delta^{11}B$ values in the Teremkyn tourmalines are the most diverse, from -15.7 to +2.5‰. Tourmaline core compositions yield an inferred $\delta^{11}B$ value of the initial fluid ofca. -12‰, suggesting granitic rocks as the B source, whereas the heavier rims and late-stage grains reflect Rayleigh fractionation. The $\delta^{11}B$ values of tourmaline from Talatuiare -5.2 to -0.9‰. Taking into account fluid inclusion temperatures from vein quartz (ca. 400°C), the inferred $\delta^{11}B$ value of fluid is heavy (-2.5 to +2.2‰) suggests a B source from the host metagabbro. At the Darasun deposit, tourmaline from the breccia pipe is isotopically uniform ($\delta^{11}B$ -6 to -5‰) and suggested to have precipitated from a ^{10}B-depleted, residual fluid derived from granitic rocks. The Darasun vein-hosted tourmalines I and II ($\delta^{11}B$ from -4.4 to +1.5‰) may have crystallized from strongly fractionated residual granitic fluid although mixing with heavy boron from the metagabbro rocks probably occurred as well; the boron isotopic composition of

tourmaline III (-11.2‰) is attributed to a less-fractionated fluid, possibly a recharge from the same source.

Introduction

The use of tourmaline-supergroup minerals as a geochemical tool in ore deposit research is well established (e.g. Taylor and Slack 1984; Palmer and Slack 1989; Rozendaal and Bruwer 1995; Slack 1996; Jiang et al. 1999; Torres-Ruiz et al. 2003; Raith et al. 2004; Xavier et al. 2008; Pal et al. 2010; Trumbull et al. 2011; Slack and Trumbull 2011). This paper is focused on variations of chemical and B isotopic compositions of tourmalines from three hydrothermal gold deposits in the Darasun district, Transbaikal region, Russia. These include Darasun proper (the largest, with ~3.5 MOz Au), Teremkyn (~353 kOz Au), and Talatui (~1.1 MOz Au). Previous studies of the Darasun district have concentrated on the geological setting, descriptive mineralogy, and fluid inclusions of the deposits (e.g. Sakharova 1972; Timofeyevsky 1972; Lyakhov 1975; Zorina 1993; Prokof'ev and Zorina 1994; Zorin et al. 2001; Prokofiev et al. 2010, 2012; Prokof'ev et al. 2004, 2007; Spiridonov et al. 2010). Recently, Baksheev et al. (2011) studied tourmaline from quartz-carbonate veins from the Darasun deposit, with emphasis on the high proportion of ferric vs. ferrous iron determined by Mössbauer spectroscopy. They proposed a major role for the $(AlFe_{-1})$ substitution and pointed out the similarity, in this respect, to tourmaline from porphyry-type Cu and Sn deposits. Data for tourmaline are combined with constraints on mineralizing conditions from published data on fluid inclusions in associated quartz. The aim is to contribute a new understanding of fluid source(s) in the hydrothermal systems of the Darasun district and on processes that may have led to mineralization.

Geological setting

The oldest units in the Darasun gold district are meta-igneous rocks of the lower Paleozoic Kruchininsky Complex, which comprises pyroxene-hornblende-, hornblende-, and olivine-gabbro, as well as small bodies of serpentinized pyroxenite, plagioclase dunite, peridotite, troctolite, and anorthosite (Fig. 1). According to Kazimirovsky et al. (1993), these mafic and ultramafic rocks were derived from a common parental magma having a composition close to subalkaline picrite. Kazimirovsky et al. (1992) suggested that the protoliths of the mafic rocks represent oceanic crust that formed in marginal parts of the Mongolian-Okhotsk ocean in the early Paleozoic.

The Kruchininsky Complex is intruded in the southeastern part of the Darasun district by late Paleozoic diorite, granodiorite, and granitic rocks of the Krestovsky Complex (Fig. 1), which were dated by the Rb-Sr isochron method at 320-316 Ma (Rublev et al. 1985). The Krestovsky

Complex, in turn, was intruded by late Paleozoic to early Mesosoic leucogranite, granodiorite, and syenogranite of the Olyokma Complex in the northeastern and southeastern parts of the district. The Triassic Amanan intrusive complex (K/Ar age 234±8 Ma; Rublev et al. 1985) in the northwestern part of the Darasun district comprises biotite-amphibole-feldspar diorite, syenogranite, granite, and alaskite. The youngest intrusive units in the area belong to the Amudzhikan-Sretensky Complex of Middle Jurassic to Early Cretaceous age (K/Ar age 193-109 Ma; Rublev et al. 1985). This highly variable complex comprises volcanic and hypabyssal intrusive rocks with subalkaline to weakly alkaline affinities. The units include stocks and dikes of diorite and quartz-diorite porphyry; syenogranite, syenite, granite and granodiorite porphyry, dikes and flows of felsite, felsite porphyry, and obsidian; as well as flows of trachybasalt, trachyandesite, latite, trachydacite, rhyodacite, quartz porphyry, and rhyolite.

The hydrothermal ore-bearing veins in the Darasun district are controlled by brittle fracture systems that formed during the collision of the Siberian and Sino-Korean continents at160-140 Ma (Chernyshev et al. 2014). Mineralization in the veins is spatially associated with the Mesozoic intrusions of the Amudzhikan-Sretensky Complex (Zorin et al. 2001). Orebodies of the Talatui and Teremkyn deposits are hosted in mafic rocks, whereas the veins and breccias of the Darasun deposit are in felsic and mafic rocks (Fig. 1). There is no evidence for post-ore metamorphic or deformational overprint in the gold deposits.

The Darasun gold deposits
The Darasun gold deposits have been described in detail by Prokofiev et al. (2010), from which the following summary of main features is taken.

The Teremkyn deposit comprises closely-spaced, gently to steeply-dipping, gold-sulfide-tourmaline-quartz veins hosted in propylitically altered metagabbro spatially related to granodiorite porphyry of the Amudzhikan-Sretensky Complex (Fig. 1). Mineralized veins and alteration zones cut metagabbro of the Kruchinisky Complex and diorite of the Krestovsky Complex. The gold-bearing quartz veins are 30 to 1500 m long and 3 to 50 cm thick. The gold grade in ore veins varies from 5 to 1500 g/t (average 25 g/t). Ore mineral assemblages of the Teremkyn vein deposits include major pyrite and chalcopyrite, accompanied by minor sphalerite, arsenopyrite, galena, tennantite-tetrahedrite group minerals, Bi-sulfosalts, sulfotellurides, and native gold. Quartz, tourmaline, chlorite, and carbonates are the main gangue constituents.

The Talatui deposit, located 7 km northwest of Teremkyn (Fig. 1), comprises complex, irregular mineralized zones and lenses spatially related to dikes of the Amudzhikan-Sretensky Complex (diorite porphyry, lamprophyre, granodiorite and granite porphyry), which cut propylitically and potassically altered metagabbro and dikes of the Kruchinisky Complex and diorite of the Krestovsky Complex. The mineralized zones of 120 to 1400 m long and up to 10 m thick; the lenses are 150-200 m in lenght with up to 2 m in thickness. Gold grades vary from 1-

200 g/t (average 8.5 g/t). Magnetite, hematite, pyrite, and chalcopyrite are the major ore minerals; minor ore minerals include sphalerite, siegenite [$(Ni,Co)_3S_4$], glaucodot [$(Co,Fe)AsS$], cobaltite [$CoAsS$], molybdenite, native gold, matildite [$AgBiS_2$], and hessite [Ag_2Te]. Gangue constituents are quartz, tourmaline, K-feldspar, chlorite, phlogopite, and carbonates.

The Darasun deposit, 5 km southeast of Teremkyn, comprises more than 200 steeply-dipping, gold-quartz veins and pipe-shaped breccia bodies spatially related to dikes and stocks of high-K granodiorite porphyry belonging to the Amudzhikan-Sretensky Complex. The breccia pipes are localized at the margins of the granodiorite-porphyry intrusions and contain fragments of granodiorite porphyry cemented by quartz, tourmaline, and pyrite. According to Timofeyevsky (1972), this breccia fills channels in which the mineralizing fluids ascended. The Darasun gold-quartz veins are 50 to 2000 m long and 5 to 80 cm thick. The pipe-shaped breccia bodies are up to 150 m in diameter and 500 to 800 m in length. There are no cross-cutting relationships to show the geologic relationship between the breccia pipes and veins. The gold grade in the breccias pipes is up to 3.5 g/t. The major ore mineral is pyrite; gangue minerals are chiefly quartz and tourmaline, with minor calcite and fluorite. The Darasun gold-quartz veins are steeply-dipping, show propylitic and carbonate-quartz-sericite alteration zones, and cut all igneous units including metagabbro and diorite of the Kruchininsky Complex, and granitic rocks of the Olekma Complex. Gold grades in the veins range from 1.5 g/t to 1.5 kg/t (average 15.4 g/t). The major ore minerals are pyrite, arsenopyrite, chalcopyrite, sphalerite, and galena; minor phases are tennantite-tetrahedrite group minerals, Sb and Bi sulfosalts, sulfotellurides, tellurides, native gold and native arsenic. The gangue comprises quartz, tourmaline, carbonates, anhydrite and gypsum.

Previous studies

The chemical composition and possible isomorphic substitutions in tourmalines from the Darasun district in the samples 878t, 154/05, 1165, and 1185dr/86 in which boron isotopic composition was measured in this study had been previously reported by Baksheev et al. (2011, 2012) and Prokofiev et al. (2012). However, these papers did not publish the point analyses of tourmalines.

According to Baksheev et al. (2012) and Prokofiev et al. (2012), vein-hosted tourmaline from the Teremkyn deposit is classified as schorl, oxy-schorl, dravite, and oxy-dravite. The composition of the Teremkyn tourmalines evolved from Fe- and Ca-rich to Fe- and Ca-poor varieties. Tourmaline from the Talatui deposit is classified as Ca-rich oxy-dravite. The compositions of tourmalines from the both deposits follow the O-P trend (oxy-dravite--povondraite) with the major isomorphic substitution $Fe^{3+} \rightarrow Al^{3+}$. At the Darasun deposit, tourmalines occur in breccia pipes and veins. Characteristic of breccia-hosted tourmalines is a high proportion of *X*-site vacancy (Baksheev et al., 2012). This tourmaline is classified as vacancy-rich oxy-dravite or dravite. Similar to Teremkyn and Talatui, the major isomorphic

substitution in the breccia-hosted tourmaline is $Fe^{3+} \rightarrow Al^{3+}$. The vein-hosted tourmaline has been characterized in detail by Baksheev et al. (2011). The identified three generations of tourmaline are classified as oxy-dravite or povondraite (generation I), oxy-dravite (generation II), and dravite (generation III). Tourmaline I is characterized by the $Fe^{3+} \rightarrow Al^{3+}$ isomorphic substitution, whereas tourmalines II and II show $Fe \rightarrow Mg$ substitution.

The detailed information on fliud incluisions in quartz associated with tourmaline in the samples reported here is given by Prokofiev et al. (2010, 2012). Three types of fluid inclusions are distinguished by their appearance at room temperature. Type I three-phase inclusions containing a vapor bubble aqueous solution, and one or more daughter crystals, which are generally isotropic and transparent, thus probably chloride mineral(s); locally, opaque daughter minerals also occur. Type II inclusions are vapor-dominated two-phase inclusions with a thin rim of aqueous solution and an insignificant amount of liquid CO_2. The Type III two-phase liquid-dominated inclusions consist of unsaturated aqueous solution and a vapor bubble. The Type I and III inclusions predominate; Type II (vapor-rich) inclusions were found in all deposits, but inclusions of measureable size (>10 μm) were identified only at Talatui. The latter are relatively large, separate, and randomly distributed in different quartz grains so they were interpreted as primary.

According to Prokofiev et al. (2010, 2012), at Teremkyn, the Type III inclusions homogenize into the liquid phase at 346-320°C, with moderate salinities of 6.0 to 18.9 wt. % NaCl equiv. The fluid inclusions in quartz from the Talatui deposit include all three types. Type I inclusions homogenize completely at 311-397°C, by dissolution of the chloride daughter crystal. Salinities of this fluid range from 39.0 to 47.1 wt.% NaCl equiv. Vapor-dominated fluid inclusions, containing the least-saline fluid (0.9-4.8 wt.% NaCl equiv.) homogenized into the vapor phase at 292-358°C. The Type III inclusions of unsaturated aqueous solution homogenized to the liquid phase at 331-359°C and yielded salinities from 3.9 to 7.7 wt.% NaCl equiv. The breccia quartz from the Darasun deposit contains Type I and II inclusions. The Type I inclusions homogenize completely by disappearance of the vapor bubble at 314-471°C, and have fluid salinities of 39.2-50.2 wt.% NaCl equiv. The Type III inclusions homogenize at 315-376°C. Their salinities are 7.0-13.1 wt.% equiv. NaCl. The vein quartz contains only Type III inclusions, which homogenized to the liquid phase within a narrow temperature range of 371-387°C. Their salinities are 7.1-9.3 wt.% NaCl equiv., close to those of Type III inclusions from the breccia-hosted quartz.

Analytical techniques

The composition of tourmaline was determined in polished thin sections with a JEOL JSM-6480LV electron microscope at Moscow State University (analyst: V.O. Yapaskurt, Divison of Petrology) using an Inca Energy-350 energy dispersion system (EDS) and Inca Wave-500 wavelength dispersion system (WDS) (analyst: V.O. Yapaskurt, Division of Petrology, Moscow

State University). The electron microprobe was operated at an accelerating voltage of 15 kV and a beam current of 20 nA. The EDS detector was used for all elements except F, employing natural silicate reference minerals (Jarozewich 2002) for calibration. Uncertainty of single measurements of oxides does not exceed 1.5 % relative. Fluorine concentrations were measured with WDS (TAP crystal), using MgF_2 as a reference standard. The XPP (eXtended Pouchou & Pichoir) corrections were used for correction procedures (program "INCA" version 17a).

Tourmaline formulae were normalized on the basis of 15 cations exclusive Na, Ca, and K, i.e., assuming no vacancies at the tetrahedral or octahedral sites, and an insignificant content of Li (Henry et al. 1999). Charge-balance constraints were used to estimate the amounts of OH^- and O^{2-} in the V and W anion sites, although we acknowledge there are significant uncertainties with these estimates (Dutrow and Henry 2000). The calculated $O^{2-}$is preferentially assigned to the W site together with F (Henry et al. 2011). The proportions of ferric and ferrous iron are calculated from Mössbauer data reported by Baksheev et al. (2011, 2012) as explained in the data supplement. The proportion of X site vacancies ( ) was calculated using stoichiometric constraints by means of 1 – (Na + Ca + K). This permits the classification of tourmaline compositions in accordance with Henry et al. (2011). The amount of B_2O_3 was also calculated from stoichiometric constraints assuming 3 B apfu.

The complete dataset of electron-microprobe data from this study, together with corresponding boron isotope data are available in Online Resource 1, which contains only the new electron-microprobe data for the Teremkyn and Talatui tourmalines, which were not used in previous studies

Boron isotope analyses were performed on the same polished thin sections as microprobe analyses using the Cameca ims 6f SIMS instrument in Potsdam, Germany, following procedures explained in detail by Trumbull et al. (2008). Prior to analysis, samples were cleaned ultrasonically for 5 min in high-purity ethanol and then coated with a 35-nm-thick film of high-purity Au. The SIMS analyses employed a 0.8 nA, nominally 12.5 kV, $^{16}O^-$ primary beam focused to ca. 5 μm diameter on the sample surface. Each analysis consisted of 100 cycles in the peak sequence ^{10}B (2 s), and ^{11}B (1 s), after a pre-sputtering of 3 min per spot to remove the gold coating and establish equilibrium sputtering conditions. Total analysis time per spot was about 10 min. Calibration of SIMS analyses is based on natural tourmaline reference materials: Harvard Mineralogical Museum #112566 schorl and #108796 dravite (Dyar et al. 2001; Leeman and Tonarini 2001), and B4 schorl (Gonfiantini et al. 2003; Tonarini et al. 2003). Individual uncertainty for each 100-cycle analysis was 0.3-0.4 ‰ (1 s.d.). Repeat analyses of reference tourmalines during the 5-day analytical session yielded repeatability of 1 to 1.4 ‰ (1 s.d., n=12). The variation in the instrumental mass fractionation value for the three reference tourmalines was about 1.6 ‰ (Table 1), which we take as the best estimate for analytical accuracy. The boron isotope compositions are reported in $\delta^{11}B$ notation relative to reference

Tourmaline occurrence and chemical composition

Teremkyn

Tourmaline from the Teremkyn deposit (sample 878t) was sampled from quartz-carbonate-pyrite veins hosted in metagabbroic rock with propylitic (albite-actinolite-epidote-calcite) alteration. Along with tourmaline, the veins also contain fragments of actinolite and epidote crystals derived from the altered host rocks. The paragenetic sequence of gangue and ore minerals in Teremkyn deposit, according to Prokofiev et al. (2010) shows that gold (fineness of 655 to 896) precipitated after tourmaline and nearly simultaneous with pyrite, but before chalcopyrite (Fig 2a). Four tourmaline generations are distinguished for the first time: (I) relatively large (100-200 µm) isolated and brecciated grains, (II) cements and overgrowths (10-50 µm) on brecciated grains, (III) fine-grained (3-10 µm) crystals filling interstices between earlier tourmaline, and (IV) sheaf-like (100-500 µm) aggregates (Figs. 3a,b). All types are strongly pleochroic from pale yellow to dark green. Microscopic observations indicate that at Teremkyn, quartz crystallized later than tourmaline I because it contains fragments of tourmaline cemented and overgrown by tourmaline II. Tourmalines II to IV is assumed to have crystallized during the precipitation of vein quartz, because no textural evidence was found that tourmaline formed earlier. Therefore, the primary fluid inclusions in Teremkyn quartz (see above) allow evaluation of the formation conditions of tourmaline II-IV.

We found the most useful chemical features to discuss variations within and among the deposits are their Fe, Ca and Mg contents, and the proportion of *X*-site vacancies. Grains of the first-generation tourmaline, which locally appear rounded, are Fe- and Ca-rich (3.34-5.18 and 0.29-0.40 apfu, respectively) and low in Mg (0.11-1.35 apfu). The overgrowing tourmaline II has lower Fe and Ca contents (1.95-2.65 and 0.28-0.42 apfu, respectively) and higher Mg (1.51-1.75 apfu). Compared with other generations, tourmaline II is also enriched in Ti. The Fe and Ca concentrations in fine-grained tourmaline III are still lower (1.28-1.61 and 0.10-0.13 apfu, respectively), but Mg content does not change (1.57-1.60 apfu). The sheaf-like aggregates of tourmaline IV have Fe and Ca contents at the base similar to those of tourmaline II (1.96-2.67 and 0.16-0.37 apfu, respectively), whereas the tips have lower contents (1.27-1.60 and 0.11-0.17 apfu, respectively) and thus similar to tourmaline III. The Mg concentration is uniform in tourmaline IV (1.48-1.74apfu) and close to that in tourmaline II.

Talatui

Tourmaline at Talatui (sample 154) was sampled from a quartz-pyrite vein hosted in altered metagabbro. According to Prokof'ev et al. (2007), high-fineness gold (951-996) precipitated nearly simultaneous with tourmaline (Fig 2b), whereas gold with lower fineness (777-875) was deposited simultaneously with late pyrite and chalcopyrite (Fig. 2c). The tourmaline forms

isolated dark green crystals up to 200 μm long or crystal aggregates (Fig. 3c). In thin section, the tourmaline is pleochroic from light to dark green. Crystals are irregularly zoned (Fig. 3c), with higher Fe and Ca contents in dark and light zones (1.51-1.69 and 2.20-2.32 apfu vs. 0.16-0.23 and 0.28-0.30 apfu, respectively; see Online Resource 1). The high Fe and Ca compositions are similar to tourmaline II from Teremkyn, whereas their Mg content is slightly higher (Online Resource 1). In addition, the Talatui tourmaline is distinguished by the highest concentration of Ti and V among the three studied deposits.

According to microscopic observations, fragments of tourmaline crystals are cemented by quartz, calcite, and pyrite; hence, those minerals precipitated later than tourmaline .

Darasun

Tourmaline from the Darasun gold deposit was collected from a breccia pipe and from quartz veins. The vein-hosted tourmalines were the subject of a previous study by Baksheev et al. (2011). The breccia and veins are spatially isolated and therefore no relations between them can be observed. In the breccia pipe, gold is disseminated in sulfide minerals, which crystallized simultaneously with tourmaline (Fig. 2e). In the quartz veins, tourmaline precipitated with quartz and pyrite, but before the gold (Fig. 2d), which has a fineness of 590 to 896 (Prokofiev et al. 2010).

Two morphological types of tourmaline are identified in the breccia pipe: isolated crystals (50-200 μm) and sheaf-like aggregates (100-600 μm) (Fig. 3d). Both types are pleochroic from pale yellow to pale brown. The isolated crystals are compositionally zoned, with increasing Fe, Ca, and Na contents toward the rim, whereas Al and X-site vacancies decrease (see Online Resource 1). The Mg contents are variable, increasing slightly from the core to an intermediate zone then decreasing to the rim. The sheaf-like aggregates are also chemically zoned (Fig. 3d), whereby the tips of some crystals are richer in Fe than the base. The isolated grains and sheaf-like tourmaline aggregates have similar Fe and Ca contents to the vein-hosted tourmaline III (see below).

The Darasun vein-hosted tourmaline has been characterized in detail by Baksheev et al. (2011) and we provide only a brief description here. Three generations are recognized on the basis of appearance and composition. Tourmaline crystals of the first generation (I) are complexly zoned (Fig. 3e), pleochroic from pale green to dark green, and range in size from 50 to 250 μm. Tourmaline II forms 5-50 μm unzoned crystals overgrowing tourmaline I (Fig. 3f), or separate unzoned crystals. Darasun tourmaline III fills thin fractures (up to 20 μm thick) in earlier tourmalines. The Online Resource 1 contains complete electron-microprobe data of all tourmaline generations. The chemical compositions of tourmaline I show a high Fe content that is similar to that of tourmaline I from the Teremkyn deposit, although Ca is lower. Tourmaline II differs in having significantly lower Fe and Ca contents, similar to tourmaline III from Teremkyn.

Tourmaline III has low Fe and Ca contents like the breccia-hosted tourmalines, but without the high proportion of *X*-site vacancies.

In the breccia pipe at Darasun, there is no clear evidence that tourmaline and quartz crystallized at different times, thus their simultaneous crystallization is assumed. The Darasun vein-hosted tourmaline of the first and second generations crystallized before quartz, since tourmaline fragments are enclosed in the latter. Tourmaline III presumably precipitated simultaneously with quartz.

Boron isotope compositions

This study reports 56 SIMS boron isotope analyses of tourmaline from mineralized quartz veins at the Teremkyn and Talatui deposits, and from both quartz vein and breccia pipe mineralization at the Darasun deposit. The complete boron isotope dataset is given in Online Resource 2, and selected compositions of chemical and B-isotope data are reported in Table 2. The total range of $\delta^{11}B$ values from all deposits is very large, from about -15.7 to +11.2‰ (Table 2 and Fig. 4). However, important isotopic differences exist within individual deposits, relating to different generations of tourmaline growth. These differences are described in detail below and interpreted in terms of host rock composition, temperature of crystallization, fluid source, and fluid evolution.

Teremkyn

The $\delta^{11}B$ values of tourmaline from the Teremkyn deposit span the largest range in this study, from -15.7 to +2.5‰ (Fig. 4a). In detail, the boron isotopic composition of tourmaline I becomes heavier with progressive growth (Fig. 6a), from -15.7 to -9.3‰ in the cores to -7.3 to -3.2‰ in the rims. Tourmaline II (overgrowths) is isotopically lighter than generation I rims, ranging from -9.3 to -7.5‰. The $\delta^{11}B$ value of cementing tourmaline III is -5.7‰, similar again to the tourmaline I rims (Fig. 4a). Finally, the $\delta^{11}B$ values of late, sheaf-like tourmaline IV are the highest of all generations (-2.6 to +2.5 ‰), and there is a trend from heavier boron at the base to slightly lighter boron in the tips(+0.2 to +2.5‰, vs. -2.6 to -1.6‰, respectively; see Figs. 3b, 4a).

Talatui

Tourmaline from the Talatui deposit forms just one textural type and the range of $\delta^{11}B$ values is correspondingly narrow, with -5.2 to -0.9‰ (Table 2, Fig. 4a). The boron isotopic composition is close to those of tourmalines II and III from the Teremkyn deposit. The BSE image of Talatui tourmaline shows significant chemical zoning (Fig. 3c), but there is no significant difference in B-isotope ratio between cores and rims relative to the measurement uncertainty of ± 1.6‰. (Fig. 3c). Some grains display a patchy internal variation in $\delta^{11}B$ that goes beyond this uncertainty,

such as the longitudinal section shown in Figure 3c with a variation from -2.1 to -0.9‰, but this difference is 1.2 permil, which is less than uncertainty.

Darasun

Tourmalines from the breccia pipe and quartz-carbonate-pyrite veins in the Darasun deposit differ strongly in their B-isotope composition. The $\delta^{11}B$ values of tourmaline from the breccia pipe are identical, within analytical uncertainty, at -6.0 to -5.0 ‰ (n=5, see Fig. 4b). There is no internal zoning, nor any difference in isotope composition between the isolated grains and the sheaf-like aggregates. In contrast to that, the vein-hosted tourmaline displays a much wider range of $\delta^{11}B$ values, extending to both heavier and lighter values, from -11.4 to +3.8 ‰ (Fig. 4b). In detail, different tourmaline generations have smaller and distinct ranges. Multiple analyses of larger crystals of tourmaline I (Fig. 3e) yielded $\delta^{11}B$ from -0.1 to +1.5‰ with some tendency for isotopically lighter rims relative to cores, but within the ±1.6 ‰ uncertainty. Tourmaline II, represented by the tips of prismatic crystals in radial aggregates, has significantly lower $\delta^{11}B$ values (-4.4 to -3.7‰) than generation I (Figs. 3f, 4b). Finally, the fracture-filling tourmaline III has the lowest $\delta^{11}B$ value (-11.4‰). This is a single analysis from a veinlet cutting aggregates of tourmaline I and II. The veinlet also contains tourmaline fragments with $\delta^{11}B$ values from -2.4 to +1.5‰, which are consistent with tourmaline I. Two other tourmaline fragments in the veinlet have isotopically heavy boron (+3.8 and +11.2‰). The two extreme light and heavy values of -11.4 and +11.2‰ are single-point outliers on grains too small for multiple analysis. There is nothing to suggest analytical error of these points, but they should be interpreted with caution. The remaining analyses from Darasun vein tourmalines of generations I and II fall within the range of -4.4 to +3.4 ‰.

Discussion

Host-rock controls on tourmaline major-element compositions

The earliest generation of tourmaline from the quartz-carbonate-pyrite veins in altered metagabbro at the Teremkyn deposits has the highest Fe and Ca content, and the lowest Mg and Al_{tot}. Tourmaline I crystallized before vein quartz, therefore it could be contemporaneous with epidote and actinolite, whose fragments are also present in the vein. This tourmaline is thus interpreted as originating in the altered wallrock rather than in the veins. During the crystallization of tourmaline I, Mg and Al were preferentially incorporated in actinolite and epidote, rather than in tourmaline. In paragenetically later tourmalines, the concentrations of Fe and Ca are lower, possibly because of deposition of pyrite and calcite related to increasing f_{H2S} and f_{CO2} in the mineralizing fluid.

In the rather homogeneous tourmaline from the Talatui deposit, Fe and Ca contents are similar to those in tourmaline II from the Teremkyn deposit. Like at Teremkyn, the Talatui tourmaline occurs in metagabbro-hosted quartz veins containing pyrite and carbonate (Fig. 3c).

Thus we suggest that the major-element variations of tourmalines from these two deposits reflect a similar control by host-rock lithology and competition for Fe and Ca with pyrite and calcite, respectively. The local high contents of Ti and V in tourmaline can be explained by the breakdown of primary titanomagnetite in the altered metagabbro host rocks.

The Darasun breccia pipe tourmalines have very low Fe_{tot} and Ca contents relative to the tourmalines from Teremkyn and Talatui, which likely reflects the felsic host rocks of the breccia pipe (K-rich granodiorite porphyry) as well as the competition for these elements by associated pyrite and calcite. A unique feature of the breccia-hosted tourmaline is its high proportion of X-site vacancies. Usually, high proportions of the X-site vacancy in tourmaline are caused by low Na content in the fluid (van Hinsberg et al. 2011; Henry and Dutrow 2012). However, the Na concentrations in the breccia-hosted tourmalines are not significantly lower than for other tourmalines on the Darasun district regardless of their host rocks. However, these tourmalines do differ significantly in their Ca contents. Therefore, we conclude that proportion of X-site vacancies is controlled by Ca concentration rather than Na content. The Ca content, in turn, is influenced by both Ca concentration in the host rock (higher in metagabbro, lower in breccia and granodiorite at Darasun), and by the CO_2 fugacity controlling carbonate stability in the fluid.

In contrast to the breccia pipe samples, the early generation of tourmaline in the Darasun veins hosted in granodiorite porphyry has high Fe_{tot} and Ca contents like at Teremkyn and Talatui, suggesting the mineralizing fluid interacted with metagabbro in the regional country rocks. Baksheev et al. (2011) reported an increase of the Fe^{3+}/Fe_{tot} value in the first generation of tourmaline, proposing that this reflects a higher oxygen fugacity compared to later fluids. Oxidation of the fluid was suggested to have resulted from boiling, which was inferred from fluid inclusion data and would cause a loss of H_2 to the vapor phase (e.g. Yang and Jang 2002). The lower Fe_{tot} and Ca contents in later tourmaline generations II and III at the Darasun deposit are attributed here to the same effect as for Teremkyn, i.e., increasing fH_2S and fCO_2 in fluids promoting precipitation of pyrite and calcite, which sequestered Fe and Ca, respectively.

Boron isotope variations and evidence for mixed boron sources
It is important to recall the contrast in immediate host rocks in the Termkyn and Talatui deposits (metagabbro) vs. the Darasun deposit in granitoids. This contrast can have an important influence on the B-isotope composition of tourmaline because generally, the isotopic composition of boron in felsic crust (granites, gneisses, clastic metasedimentary rocks) is ca. -10‰, whereas boron in basic and ultrabasic rocks is heavier, with $\delta^{11}B$ values from -5 to +5‰, the heavier range being due to basalt-seawater interaction (Hoefs 2009; Marschall and Jiang 2011). Considering the intensity of veining and abundant hydrothermal alteration within the Darasun district, mixing of fluids from these two sources is likely. An important factor in the B-isotope systematics of hydrothermal tourmaline besides the boron source is the temperature-dependent fractionation of ^{11}B and ^{10}B between tourmaline and aqueous solution. Of two

experimental fractionation studies (Palmer et al. 1992; Meyer et al. 2008), the latter is used in this study because it better fits isotopic zoning profiles of tourmaline grown at known temperature and fluid composition (Marschall et al. 2009).

Teremkyn

There is a significant shift in boron isotopic composition from the core to rim of tourmaline I, with higher $\delta^{11}B$ values present in the rims (-15.7 to -9.3‰ vs. -7.3 to -3.2‰, respectively). Boron in tourmaline II (margin overgrowths) is isotopically lighter than that of the tourmaline I rims (-9.3 to -7.5‰) and close to the $\delta^{11}B$ value of tourmaline III (-5.7‰). Recall that tourmaline I is associated with epidote and actinolite in propylitically altered wallrock, fragments of which occur in the vein. Zharikov et al (1998) reported on the basis of combination of experiments and stabilities of characteristic propylitic minerals that propylite is formed at 200 to 350°C and epidote-actinolite- assemblage is formed at ca. 350°C. This agrees well with the range of homogenization temperatures from fluid inclusions in the Darasun district (see above and Prokofiev et al., 2010). For this temperature, the fluid-tourmaline fractionation factor of Meyer et al. (2008) is 3.2‰, resulting in a predicted B-isotope composition of -12.5‰ for the fluid precipitating tourmaline I cores. This low value would suggest a source of boron in felsic rocks like the regional granitoids. The contrast in $\delta^{11}B$ values between the core and rim of tourmaline I is on the order of 6‰, which is much larger than any reasonable cooling effect since a 50°C difference affects the fractionation factor by only 0.5‰ (Meyer et al., 2008). A likely cause is the Rayleigh fractionation effect where B-removal from fluid to form tourmaline is coupled with a progressive ^{10}B-depletion. Rayleigh fractionation curves (Fig. 5) calculated for 350°C and an initial fluid composition of -12.5‰ (based on $\delta^{11}B$ of -15.7‰ for tourmaline I core) show that the observed isotopic shift from core to rim compositions in tourmaline I would require 70-80% removal of B from the fluid. The boron isotopic composition of tourmaline II overgrowths is lighter than tourmaline I rims, which can be explained by crystallization from a less-fractionated fluid, possibly a recharge from the same source. Petrographic evidence suggests that tourmaline II was cogenetic with deposition of the vein quartz, for which fluid inclusion temperatures are ca. 330°C (see above). For this temperature, a predicted B-isotope composition of the hydrothermal fluid based on Meyer et al. (2008) is -5.9‰ (using the lowest value of -9.3‰). It is not possible to distinguish if this represents a granite-derived fluid affected by Rayleigh fractionation during formation of earlier tourmaline, or if there was mixing of heavier boron from the metagabbro. High contents of Ca in this tourmaline support the latter interpretation. Tourmaline III forming anhedral cement surrounding tourmaline I and II, has a B-isotope composition similar to the tourmaline I rim and slightly heavier that tourmaline II. Taking into account the isotopically heavier boron in this tourmaline compared with tourmaline II, we suggest that tourmaline III precipitated from the same fluid, which underwent further fractionation and loss of ^{10}B due to tourmaline precipitation according to the Rayleigh model. In

contrast to the isolated tourmaline grains just described, the sheaf-like aggregates of tourmaline IV display a narrower range of B-isotope compositions at the heavy end of the total range for the Teremkyn deposit, and the $\delta^{11}B$ values become progressively lighter towards the tips of separate crystals within the aggregates. With reference to the Rayleigh model (Fig. 5), the heavy B-isotope base of the aggregates is consistent with further fluid evolution after crystallization of tourmaline II and III. The shift back to more negative values at the tip could be fresh fluid recharge, like the shift from tourmaline II to III. A contributing factor to the isotope variations could be fluid boiling, for which there is evidence in quartz-hosted fluid inclusions, but limited experimental studies of B-isotope partitioning between aqueous fluid and vapor at 400°C indicate that the effect is 1‰ or less (Spivack et al. 1990; Liebscher et al. 2005).

The Teremkyn deposit is hosted in metagabbro and the high Ca content of tourmaline suggest a host-rock influence. However, the isotopically light boron in the early and dominant tourmaline generation I argues for a boron source derived from a granitic source. Therefore, we suggest that the initial hydrothermal fluid in the Teremkyn hydrothermal veins was derived from granitic rocks in the vicinity (Fig. 1). The heavier B-isotope composition of later tourmalines within these veins can be explained by Rayleigh fractionation of the granite-sourced fluid as explained on Figure 5, but mixing with heavy B leached from the altered metagabbro host rocks, as suggested by the high Ca contents, is also possible.

Talatui

In general, the B-isotopic composition of tourmaline from the Talatui deposit is in the same range as that of tourmaline II from Teremkyn The fluid inclusion homogenization temperature determined from associated quartz is about 400°C, yielding estimates for $\delta^{11}B$ of -2.5 to +2.2‰ in the mineralizing fluid. Taking into account that quartz postdates tourmaline in the veins, the crystallization temperature of tourmaline may be higher than the precipitation temperature of quartz, but even a temperature increase of 100°C will shift the calculated fluid $\delta^{11}B$ values to -3.3 to +1.0‰. Thus, we can conclude that the boron isotopic composition of hydrothermal fluid at Talatui is much heavier than at Teremkyn and consistent with a B source from host metagabbro. The Rayleigh model developed for Teremkyn tourmalines (Fig. 5) shows that isotopically heavy boron can result from extensive fractionation of granite-derived fluid and this cannot be ruled out but there is no evidence for an earlier, isotopically lighter tourmaline in this deposit, as was observed at the Teremkyn deposit. The BSE images of tourmalines testify to a more or less homogeneous chemical composition, and the $\delta^{11}B$ values from multiple analyses within single grains also show a uniform composition.

Darasun

Both the sheaf-like tourmaline aggregates and the isolated tourmaline crystals from the breccia pipe at the Darasun deposit have a homogeneous boron isotopic composition of -6.0 to -5.0‰.

Quartz-hosted fluid inclusions from the breccia suggest a trapping temperature of ca. 380°C, hence the δ^{11}B value of the source fluid is calculated to be about -3 to -2‰ (Meyer et al. 2008). As argued above, this relatively heavy B-isotope composition is consistent with B leached from the metagabbros or from extensive Rayleigh fractionation of isotopically lighter boron due to precipitation of earlier tourmaline. Because the breccia pipe is hosted in granitic rocks, and the boron isotopic composition of tourmalines is similar to that of generations II and III from Teremkyn, we propose the same mechanism to explain the B-isotope composition, i.e. by crystallized from a fractionated fluid derived from granitic host rocks.

The B-isotopic compositions of vein-hosted tourmaline generations I and II overlap within error, with δ^{11}B values of -0.1 to +1.5‰ and -4.4 to -1.1‰, respectively. Both ranges are heavy, similar to tourmaline compositions from the Talatui deposit and later generations of Teremkyn tourmaline. The fluid inclusion homogenization temperature of about 380°C implies a δ^{11}B fluid composition of +2.8 to +4.4‰ for generation I using the fractionation factors of Meyer et al. (2008).

The boron isotopic composition of tourmaline III (-11.4‰) is unlike any other value determined for the Darasun deposit. This value represents a single point analysis, but there is no reason to dismiss it as an analytical artifact, so if real, it must record influx of an external fluid. The two positive values of +3.8 and +11.2‰ measured from tourmaline fragments in the veinlet could be related to a continuation of the Rayleigh fractionation trend towards isotopically heavier B represented by tourmaline I and/or II, but given the large range in these single-point results and the lack of repeat analyses, any interpretation has an element of speculation.

Summarizing the isotopic results, the B-isotope composition of tourmalines from the Darasun gold district covers a very wide range from -15.7 to +11.2‰, with distinctive differences among the three deposits and an uncertain significance of the two extreme outliers. The Teremkyn tourmalines are isotopically complex and suggest mixing of at least two boron sources. One, with a light isotope composition of around -12‰ (Fig. 9) is likely to represent fluid derived from, or interacted with, granitic rocks, and then affected by variable amounts of isotopic fractionation due to tourmaline crystallization. The other, heavy boron source is fluid from alteration of metagabbro, as suggested by the high Ca contents of isotopically heavy tourmaline. The homogeneous and heavy B-isotope composition of tourmaline from the Talatui deposit suggests a B source from the host metagabbro. Tourmalines from the Darasun deposit are complex: the breccia pipe tourmaline is suggested to have crystallized from a ^{10}B-depleted, residual fluid derived from granitic rocks, whereas the vein-hosted tourmaline I and II crystallized from fluid fractionated fluid derived from granitic rocks that likely mixed with the gabbro-derived fluid; tourmaline III is formed from a less-fractionated fluid, possibly a recharge from the same source.

Conclusions

Tourmaline is a common gangue mineral in the gold deposits of the Darasun district (Teremkyn, Talatui and Darasun) in the Transbaikal region of Russia. Chemical and B-isotope compositions of this tourmaline show considerable variation, which we attribute to host-rock type (metagabbro vs. granitoid) as well as to fluid source, evolution, and temperature. Vein-hosted tourmalines from hydrothermally altered metagabbro at Teremkyn and Talatui are most commonly oxy-dravite, but there are some dravite and schorl. At the Darasun deposit, tourmaline from a breccia pipe at the margin of a granodiorite porphyry is oxy-dravite or dravite having the highest concentration of X-site vacancies of all tourmalines studied. The Darasun vein-hosted tourmaline in granodiorite evolved from a first generation of ferric-rich oxy-dravite−povondraite through a second-generation of oxy--dravite to a third-generation of dravite. The major element variations and associated minerals indicate that the chemical composition of these tourmalines was influenced by major element composition of the host rocks as well as by fluid fH_2S, fCO_2 (co-precipitation of sulfide and carbonate), and to some extent by fluid immiscibility (boiling) that affected fO_2. The boron isotopic composition of tourmaline from the Darasun gold district as a whole covers a very wide range from -15.7 to +11.2‰. This range is influenced by interaction of granite-derived hydrothermal fluid with host rocks, and by Rayleigh fractionation related to progressive crystallization of tourmaline. Our study shows that the Teremkyn tourmalines crystallized from fluid derived from granitic rocks, possibly mixed with boron derived from metagabbro as suggested by high Ca contents of the tourmaline. Homogeneous $\delta^{11}B$ values of tourmaline from the Talatui deposit suggest a boron source from the host metagabbro. Boron isotope values of tourmalines from the Darasun deposit suggest that the breccia pipe tourmaline precipitated from a ^{10}B-depleted, residual fluid derived from granitic rocks. The vein-hosted tourmalines may have crystallized from strongly fractionated residual granitic fluid although mixing with heavy boron from the metagabbro rocks probably occurred as well.

Acknowledgements

References

Baksheev IA, Prokof'ev VYu, Yapaskurt VO, Vigasina MF, Zorina LD, Solov'ev VN (2011) Ferric-iron-rich tourmaline from the Darasun gold deposit, Transbaikalia, Russia. Can Mineral 49:263-276

Baksheev IA, Prokof'ev VYu, Zaraisky GP, Chitalin AF, Yapaskurt VO, Nikolaev YN, Tikhomirov PL, Nagornaya EV, Rogacheva LI, Gorelikova NV, Kononov OV (2012) Tourmaline as a prospecting guide for the porphyry-style deposits. Eur J Mineral 24:957-979

Chernyshev IV, Prof'ev VYu, Bortnikov NS, Chugaev AV, Gol'tsman YuV, Lebedev VA, Larionova YuO, Zorina LD (2014) Age of porphyry granodiorite and berezite of the Darasun goldfield, Eastern Transbaikal region, Russia. Geo Ore Dep 56:3-12

Dutrow BL, Henry DJ (2000) Complexly zoned fibrous tourmaline, Cruzeiro mine, Minas Gerais, Brazil: a record of evolving magmatic and hydrothermal fluids. Can Mineral 38:131-143

Dyar MD, Wiedenbeck M, Robertson D, Cross LR, Delany JS, Ferrguson K, Francis CA, Grew S, Guidotti CV, Hervig RL, Hughes JM, Husler J, Leeman WP, McGuire A, Rhede D, Rothe H, Paul RL, Richards I, Yates M (2001) Reference minerals for microanalyses of light elements. Geostandards Newslett 25:441-463

Gonfiantini R, Tonarini S, Gröning M, Adorni-Braccesi A, Al-Ammar AS, Astner M, Bächler S, Barnes RM, Basset RL, Cocherie A, Deyhle A, Dini A, Ferrara G, Gaillardet J, Grimm J, Guerrot C, Krähenbühl U, Layne L, Lemarchand D, Meixner A, Northington DJ, Pennisi M, Reitznerová E, Rodushkin I, Sugiura N, Surberg R, Tonn S, Wieddenbeck M, Wunderli S, Xiao Y-K, Zack T (2003) Intercomparison of boron isotope and concentration measurements. II. Evaluation of results. Geostandards Newslett 27:41-57

Henry DJ, Kirkland BL, Kirkland DW (1999) Sector-zoned tourmaline from the cap rock of a salt dome. Eur J Mineral 11:263-280.

Henry DJ, Novák M, Hawthorne FC, Ertl A, Dutrow BL, Uher P, Pezzotta F (2011) Nomenclature of the tourmaline-supergroup minerals. Am Mineral 96:895-913

Henry DJ, Dutrow BL (2012) Tourmaline at diagenetic to low-grade metamorphic conditions: Its petrologic applicability. Lithos 154:16-32

van Hinsberg VJ, Henry DJ, Dutrow BL (2011) Tourmaline as a petrologic forensic mineral: A unique recorder of its geologic past. Elements 7:327-332

Hoefs J (2009) Stable isotope geochemistry. 6th Edition. Springer-Verlag, Berlin-Heildelberg, 285 pp

Jarozewich E (2002) Smithsonian microbeam standards. J Res Natl Inst Stand Technol 107:681-685

Jiang S-Y, Palmer MR, Slack JF, Shaw, DR (1999) Boron isotope systematics of tourmaline formation in the Sullivan Pb–Zn–Ag deposit, British Columbia, Canada. Chem Geol 158:131–144

Kazimirovsky ME, Plyusnin GS, Smirnov VN, Fefelov NN (1992) Geochemical features and isotopic age of the rocks from the core of the Darasun tectonomagmatic structure. Russian Geol Geophys 33:35-70 (in Russian)

Kazimirovsky ME, Zorina LD, Kulikova ZI (1993) The evolution of Paleozoic ultramafic and mafic magmatism of the Darasun ore district. Otechestv Geol 9:54-60 (in Russian)

Leeman WP, Tonarini S (2001) Boron isotopic analysis of proposed borosilicate mineral reference samples. Geostandards Newslett 25:399-403

Liebscher A, Meixner A, Romer RL, Heinrich W (2005) Liquid-vapor fractionation of boron and boron isotopes: experimental calibration at $400^{\circ}C/23$ MPa to $450^{\circ}C/42$ MPa. Geochim Cosmochim Acta 69:5693-5704

Lyakhov YuV (1975) Temperature zonation in the Darasun deposit. Geol Rudn Mestorozhd 17:28-36 (in Russian)

Marschall HR, Jiang SY (2011) Tourmaline isotopes: no element left behind. Elements 7:313-320

Marschall HR, Meyer C, Wunder B, Ludwig T, Heinrich W (2009) Experimental boron isotope fractionation between tourmaline and fluid: confirmation from in situ analyses by secondary ion mass spectrometry and from Rayleigh fractionation modeling. Contrib Mineral Petrol 158:675-681

Meyer C, Wunder B, Meixner A, Romer RL, Heinrich W (2008) Boron-isotope fractionation between tourmaline and fluid: an experimental re-investigation. Contrib Mineral Petrol 156:259-267

Pal, DC, Trumbull, R, Wiedenbeck, M (2010) Chemical and boron isotope compositions of tourmaline from the Jaduguda U (-Cu-Fe) deposit, Singhbhum shear zone, India: implications for the source and evolution of the mineralizing fluid. Chem Geol 277: 245-260

Palmer MR, London D, Morgan GB, Babb HA (1992) Experimental determination of fractionation of $^{11}B/^{10}B$ between tourmaline and aqueous vapor: a temperature and pressure dependent isotopic system. Chem Geol (Isotope Geosci Sect) 101:123-130

Palmer MR, Slack JF (1989) Boron isotopic composition of tourmaline from massive sulfide deposits and tourmalinites. Contrib Mineral Petrol 103:434-451

Prokof'ev VYu, Zorina LD (1994) Evolution of fluids of the Darasun ore-magmatic system (eastern Transbaikal region). Doklady Akad Nauk 335:206-209 (in Russian)

Prokof'ev VYu, Zorina LD, Baksheev IA, Plotinskaya OYu, Kudryavtseva OE, Ishkov YuM (2004) Minerals and formation conditions of ores of the Teremkin gold deposit (eastern Transbaikal region). Geol Ore Deposits 46:332-352

Prokof'ev VYu, Zorina, LD, Kovalenker, VA, Akinfeev, NN, Baksheev, IA, Krasnov, AN, Yurgenson, GA, Trubkin, NV (2007) Composition, formation conditions, and genesis of the Talatui gold deposit, the eastern Transbaikal region. Geol Ore Deposits 49:31-68

Prokofiev VYu, Garofalo PS, Bortnikov NS, Kovalenker VA, Zorina LD, Grichuk DV, Selektor SL (2010) Fluid inclusion constraints on the genesis of gold in the Darasun district (eastern Transbaikalia) Russia. Econ Geol 105:395–416

Prokofiev, V, Baksheev, I, Zorina, L, Belyatsky, B, Ustinov, V, Krivitskaya, N (2012) Tourmalinization at the Darasun goldfield, Eastern Transbaikalia: Compositional, fluid inclusion and isotopic constraints. Geoscience Frontiers, 3:59-71.

Raith JG, Riemer N, Meisel ST (2004) Boron metasomatism and behaviour of rare earth elements during formation of tourmaline rocks in the eastern Arunta Inlier, central Australia. Contrib Mineral Petrol 147:91-109

Rozendaal A, Bruwer L (1995) Tourmaline nodules: indicators of hydrothermal alteration and Sn-Zn-(W) mineralization in the Cape Granite Suite, South Africa. J African Earth Sci 21:153-167

Rublev AG, Aleksandrov GV, Aleksandrova SV, Murina GA, Shergina YuP (1985) Geochronology of the Phanerozoic activation magmatism of the southeastern Transbaikal region. Soviet Geol 10:81-92 (in Russian)

Sakharova MS (1972) Stages of ore formation and zoning of the Darasun gold deposit. In: Ivensen YuP (ed) Ore formation and its relation to magmatism. Nauka, Moscow, pp. 213-222 (in Russian)

Slack JF (1996) Tourmaline associations with hydrothermal ore deposits. In:Grew ES, Anovitz LM (eds) Boron:mineralogy, petrology andgeochemistry. RevMineral 33:559-644

Slack JF, Trumbull RB (2011) Tourmaline as a recorder of ore-forming processes. Elements 7:321–326

Spiridonov AM, Zorina LD, Letuniov SP, Prokofiev VYu (2010) The fluid regime of ore formation in the Balei gold-bearing ore-magmatic system (eastern Transbaikalia, Russia). Russian Geol Geophys 51:1102-1109

Spivack AJ, Berndt, ME, Seyfried, WE Jr (1990) Boron isotope fractionation during supercritical phase separation. Geochim Cosmochim Acta 54:2337-2339

Taylor BE, Slack JF (1984) Tourmalines from Appalachian-Caledonian massive sulfide deposits: textural, chemical, and isotopic relationships. Econ Geol 79:1703-1726

Timofeyevsky DA (1972) Geology and mineralogy of the Darasun gold area. Nedra, Moscow, 260 pp (in Russian)

Tonararini S, Pennisi M, Adorrni-Braccesi A, Dini A, Ferrara G, Gonfiantini R, Wiedenbeck M, Gröning M (2003) Intercomparison of boron isotope and concentration measurements. I. Selection, preparation and homogeneity tests of the intercomparison materials. Geostandards Newslett27:21-39

Torres-Ruiz J, Pesquera A, Gil-Crespo PP, Velilla N (2003) Origin and petrogenetic implications of tourmaline-rich rocks in the Sierra Nevada (Betic Cordillera, southeastern Spain). Chem Geol 197:55-86

Trumbull RB, Slack JF, Krienitz M-S, Belkin HE, Wiedenbeck M (2011) Fluid sources and metallogenesis in the Blackbird Co–Cu–Au–Bi–Y–REE district, Idaho, U.S.A.: insights from major-element and boron isotopic compositions of tourmaline. Can Mineral 49:225-244

Xavier RP, Wiedenbeck M, Trumbull RB, Dreher AM, Monteiro LVS, Rhede D, de Araújo CEG, Torresi I (2008) Tourmaline B-isotopes fingerprint marine evaporites as the source of high

salinity ore fluids in iron oxide-copper-gold deposits, Carajás mineral province (Brazil). Geology 36:743–746

Yang K, Jang J-Y (2002) Geochemistry of tourmalines in the Ilgwang Cu-W breccia-pipe deposit, southeastern Gyeongsang basin. J Petrol Soc Korea 11:259–270

Zharikov VA, Rusinov VL, Marakushev AA, Zaraiskii GP, Omel'yanenko BI, Pertsev NN, Rass IT, Andreeva OV, Abramov SS, Podlesskii KV (1998) Metasomatism and metasomatic rocks. Nauchny Mir, Moscow, 492 pp (in Russian)

Zorin YuA, Zorina LD, Spiridonov AM, Rutshtein IG (2001) Geodynamic setting of gold deposits in eastern and central Trans-Baikal (Chita region, Russia). Ore Geol Rev 17:215-232

Zorina LD (1993) Formation model of gold deposits in the tectonomagmatic central type structures. Russian Geol. Geophys. 34:77-83 (in Russian)
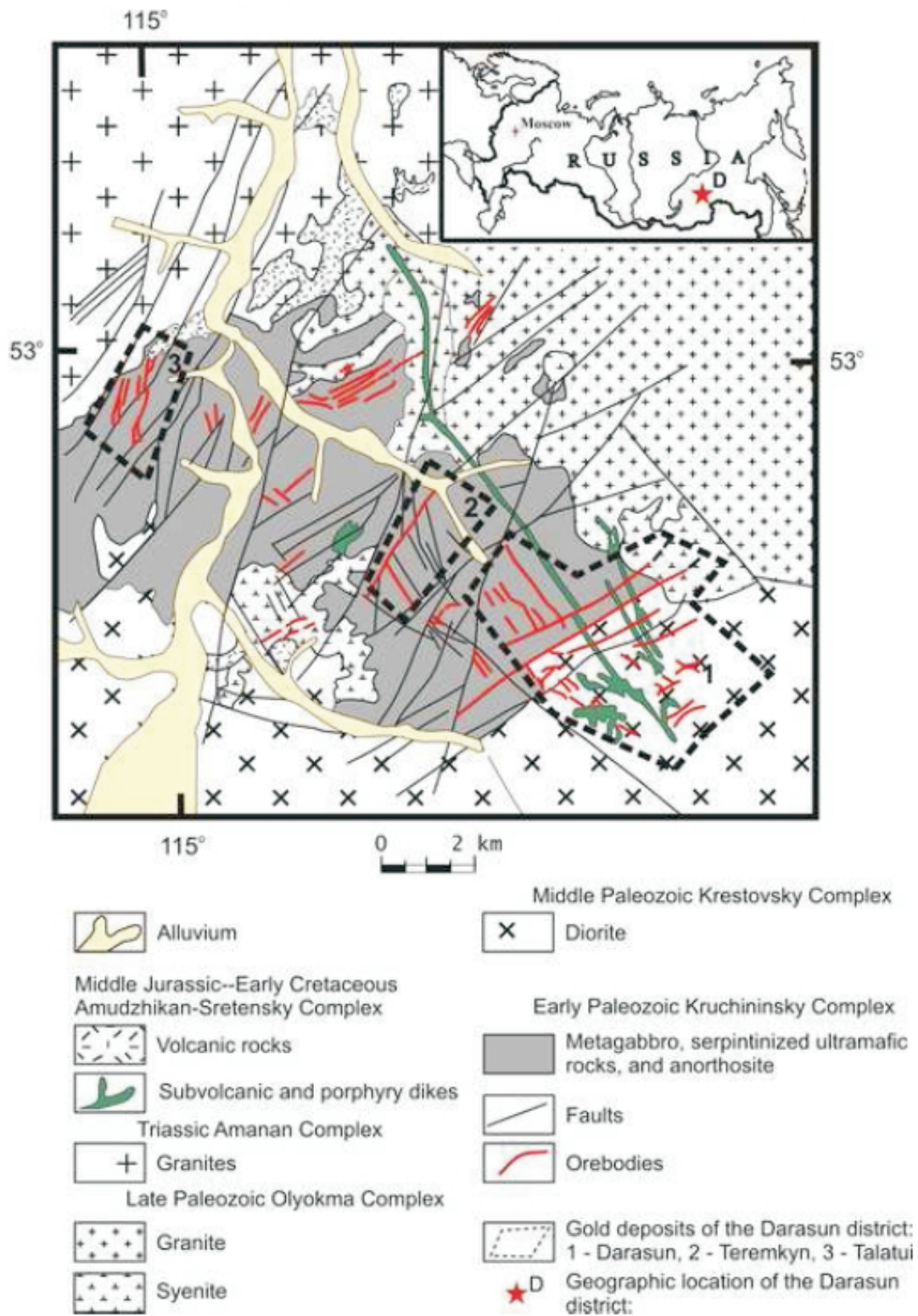
Figure Captions

Fig. 1. Geological structure of the Darasun gold district and location of the gold deposits studied here. Modified after the data of the Darasun Geological Exploration Expedition

Fig. 2. Photomicrographs of showing relationships between tourmaline, sulfide minerals, magnetite, and native gold in the ores of the Darasun district: **a** Pyrite and native gold overgrow tourmaline and in turn are overgrown by chalcopyrite, Teremkyn deposit. **b** High-fineness native gold embedded and intergrown with magnetite, Talatui deposit. **c** Low-fineness native gold embedded in chalcopyrite that contains inclusions of tourmaline, Talatui deposit. **d** Aggregate of pyrite, galena, chalcopyrite, and native gold in vein at the Darasun deposit; galena overgrowing chalcopyrite contains inclusions of tourmaline and is overgrown by native gold. **e** Gold-bearing pyrite in tourmaline-quartz matrix in the breccia of the Darasun deposit. *Au* native gold; *Chp* chalcopyrite; *Gn* galena; *Kfs* K-feldspar; *Mt* magnetite; *Py* pyrite; *Qtz* quartz; *Tu* tourmaline
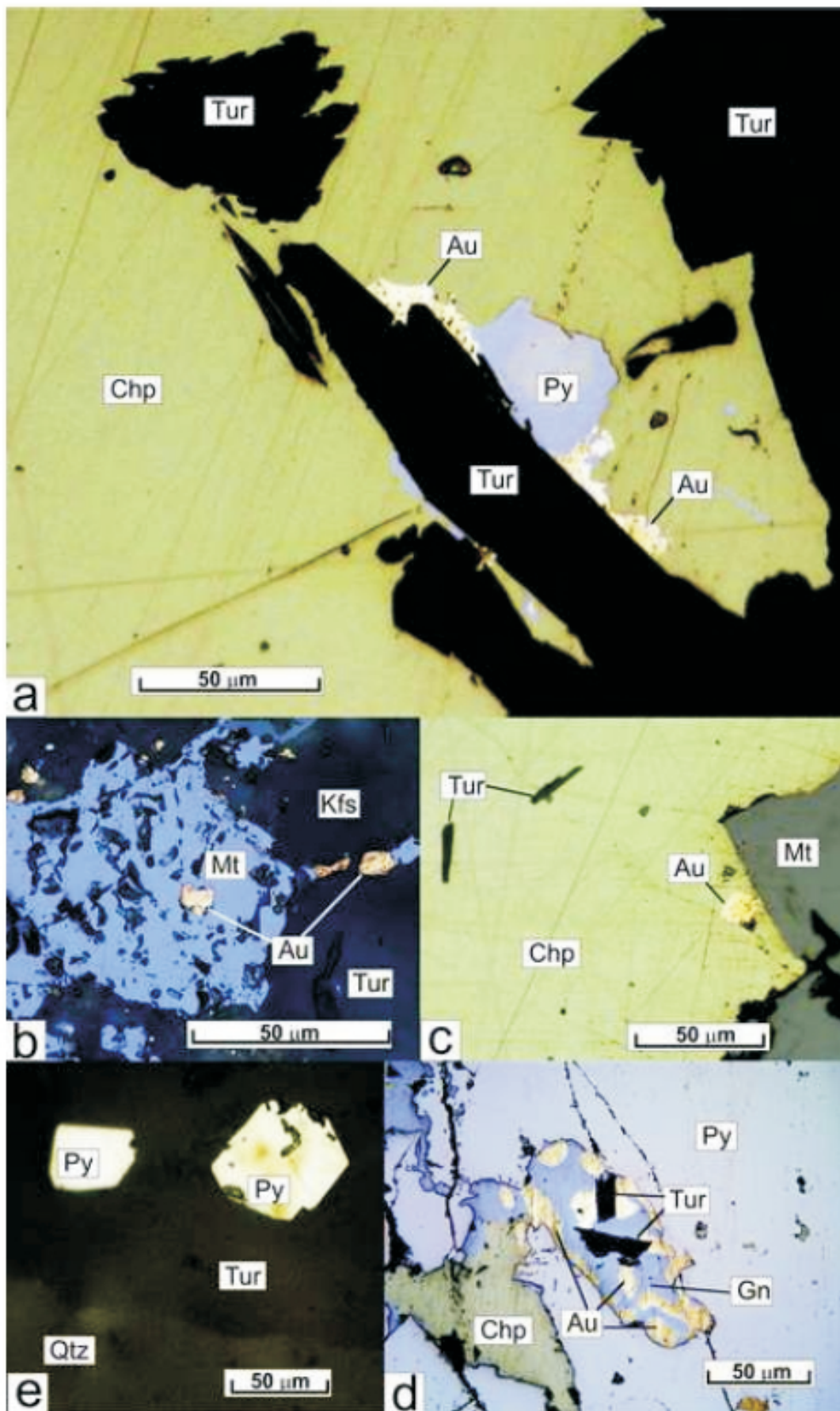
Fig. 3. BSE images of tourmaline from the Darasun gold district. Numbers denote $\delta^{11}B$ values. **a, b** Teremkyn deposit: **a** I-III generation crystals, **b** IV generation sheaf-like aggregate. **c** Crystals from the Talatui deposit. **d-f** Darasun deposit: **d** large crystal and sheaf-like aggregate from the breccia pipe, numbers in circles correspond to analyzed points listed in Fig. 5, **e** complexly zoned crystals of tourmaline I, **f** unzoned tourmaline II overgrowimg tourmaline I. *Cal* calcite; *Mus* muscovite; *Py* pyrite; *Qtz* quartz; *Tu* tourmaline; I-IV generation of tourmaline

Fig. 4. Histograms of boron isotopic composition of tourmalines from the Darasun gold district: (a) Teremkyn and Talatui deposit, (b) Darasun deposit

Fig. 5. Rayleigh fractionation models for the $\delta^{11}B$ evolution of tourmaline and equilibrated fluid of the Teremkyn deposit. Shaded boxes along the Y-axis show the observed isotopic ranges obtained from this study: (I-IV) tourmaline generations: (I core, I rim) cores and rims of large brecciated crystals, respectively; (II) overgrowing margins; (III) cement; (IV inter. part, IV tip) intermediate parts and tips of separate needles in sheaf-like aggregate, respectively

Legend

Alluvium

Middle Jurassic--Early Cretaceous Amudzhikan-Sretensky Complex
- Volcanic rocks
- Subvolcanic and porphyry dikes

Triassic Amanan Complex
- Granites

Late Paleozoic Olyokma Complex
- Granite
- Syenite

Middle Paleozoic Krestovsky Complex
- Diorite

Early Paleozoic Kruchininsky Complex
- Metagabbro, serpintinized ultramafic rocks, and anorthosite
- Faults
- Orebodies

Gold deposits of the Darasun district: 1 - Darasun, 2 - Teremkyn, 3 - Talatui

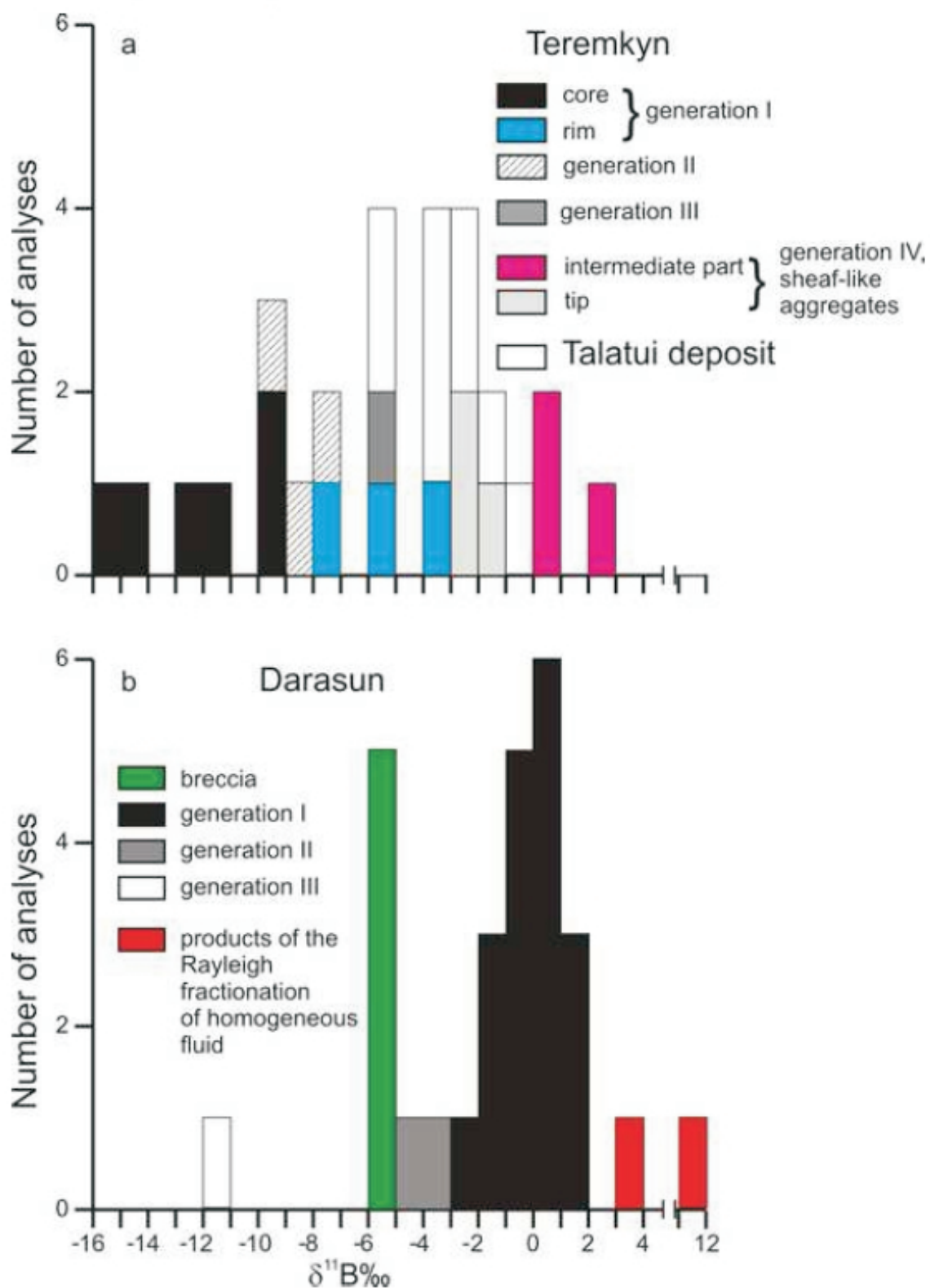D Geographic location of the Darasun district:

Baksheev Fig. 1
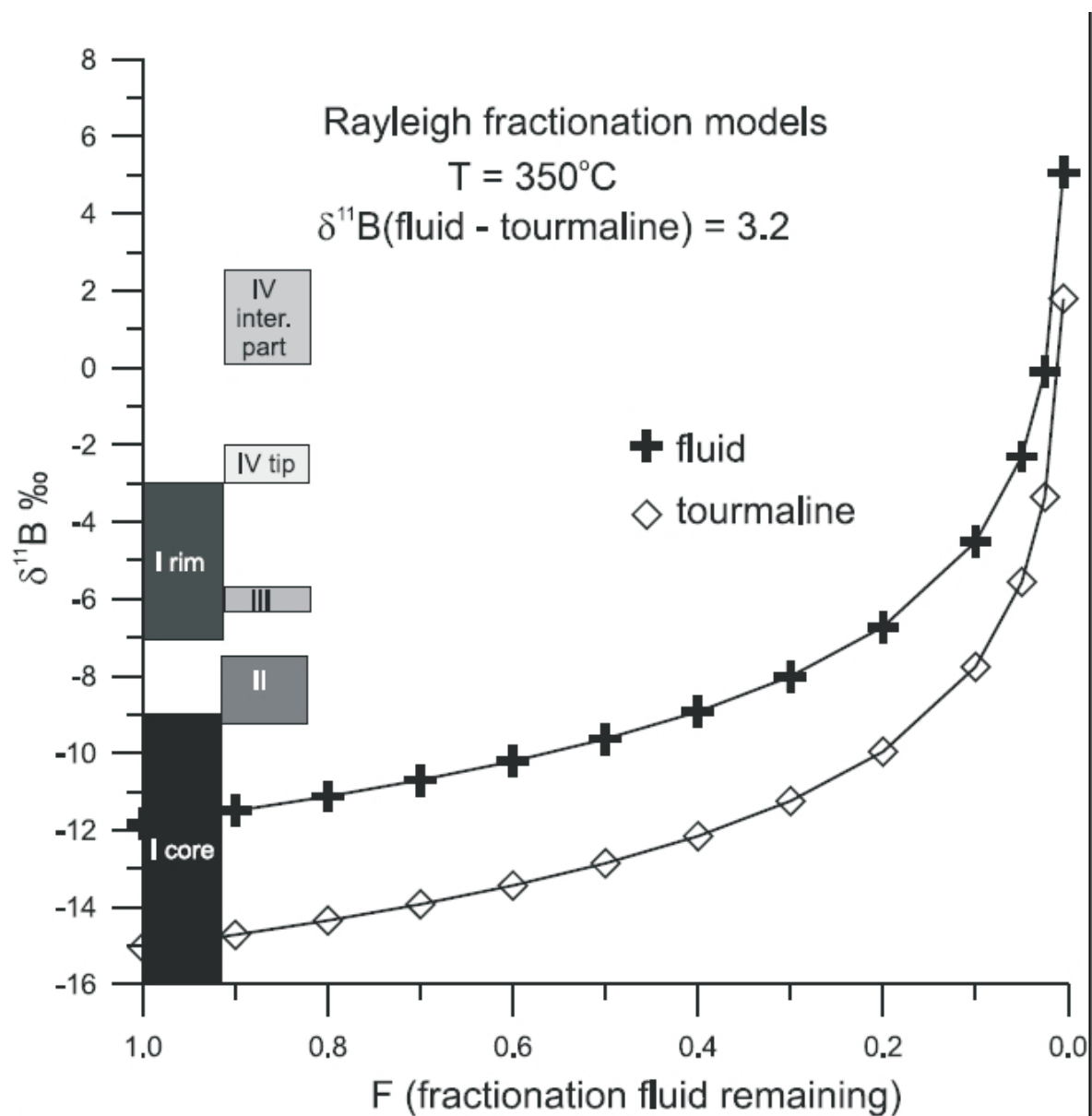
Baksheev Fig. 2

Baksheev Fig. 3

Baksheev Fig. 4

Baksheev Fig. 5

Table 1. Results of SIMS B-isotope analyses on reference tourmalines

Analysis date	$^{11}B/^{10}B$	1σ (‰) [a]	IMF [b]	$\delta^{11}B$(‰)[c]
Schorl ($^{11}B/^{10}B$ = 3.993 and $\delta^{11}B$ = -12.5)				
23-Jun-11	3.847	0.29	0.96341	-13.7
23-Jun-11	3.843	0.30	0.96241	-14.7
23-Jun-11	3.849	0.34	0.96391	-13.2
23-Jun-11	3.842	0.30	0.96216	-15.0
24-Jun-11	3.845	0.31	0.96291	-14.2
28-Jun-11	3.842	0.32	0.96216	-15.0
29-Jun-11	3.852	0.30	0.96466	-12.4
29-Jun-11	3.854	0.31	0.96516	-11.9
29-Jun-11	3.851	0.31	0.96441	-12.7
30-Jun-11	3.845	0.32	0.96291	-14.2
30-Jun-11	3.845	0.28	0.96291	-14.2
30-Jun-11	3.844	0.33	0.96266	-14.5
Mean			0.96331	-13.8
Repeatability in permil[d]			1.05	
Dravite ($^{11}B/^{10}B$ = 4.017 and $\delta^{11}B$ = -6.6)				
23-Jun-11	3.870	0.28	0.96343	-7.8
23-Jun-11	3.880	0.36	0.96592	-5.2
23-Jun-11	3.878	0.32	0.96542	-5.7
24-Jun-11	3.877	0.37	0.96517	-6.0
24-Jun-11	3.865	0.34	0.96218	-9.1
28-Jun-11	3.878	0.30	0.96542	-5.7
29-Jun-11	3.87	0.36	0.96343	-7.8
29-Jun-11	3.88	0.34	0.96492	-6.3
30-Jun-11	3.880	0.31	0.96592	-5.2
30-Jun-11	3.881	0.36	0.96617	-5.0
30-Jun-11	3.873	0.30	0.96418	-7.0
30-Jun-11	3.868	0.30	0.96293	-8.3
Mean			0.96459	-6.6
Repeatability in permil[d]			1.37	
B4 tourmaline ($^{11}B/^{10}B$ = 4.0078 and $d^{11}B$ = -8.9)				
23-Jun-11	3.863	0.36	0.96387	-9.6
23-Jun-11	3.866	0.32	0.96462	-8.8
23-Jun-11	3.872	0.31	0.96612	-7.3
24-Jun-11	3.875	0.35	0.96686	-6.5
24-Jun-11	3.867	0.35	0.96487	-8.6
28-Jun-11	3.875	0.33	0.96686	-6.5
29-Jun-11	3.871	0.34	0.96587	-7.5
29-Jun-11	3.875	0.29	0.96686	-6.5
30-Jun-11	3.874	0.29	0.96662	-6.8
30-Jun-11	3.875	0.31	0.96686	-6.5
30-Jun-11	3.872	0.29	0.96612	-7.3
Mean			0.96596	-7.4
Repeatability in permil[d]			1.09	

a) Internal precision for 100 cycles (standard deviation / mean)*1000
b) Instrumental mass fractionation ($^{11}B/^{10}B$ measured / $^{11}B/^{10}B$ standard)
c) Calculated after correction for average IMF value of all runs (0.96458)
d) Repeatability from multiple analyses of each standard (standard deviation / mean)*1000

Table 2. Summary of boron isotope composition of tourmaline from the Darasun gold district

Sample	Host and type of crystal	$\delta^{11}B$ (‰)	Number analyses	Std. dev. (‰)
	Teremkyn			
878t	Vein. Generation I, core	-15.7 to -9.3	6	2.5
	Vein. Generation I, rim	-7.3 to -3.2	3	2.1
	Vein. Generation II	-9.3 to -7.5	3	0.9
	Vein. Generation III	-5.7	1	
	Vein. Generation IV, sheaf-shaped aggregate, intermediate part	+0.2 to +2.5	2	1.6
	Vein. Generation IV, sheaf-shaped aggregate, tip	-2.6 to -1.6	4	0.5
	Talatui			
154/05	Vein. Isolated	-5.2 to -0.9	9	1.5
	Darasun			
1165	Breccia. Isolated and sheaf-shaped aggregate	-6 to -5	5	0.4
1185dr /86	Vein. Generation I	-0.9 to +1.5	14	0.8
	Vein. Generation II	-4.4 to -1.1	6	1.3
	Vein, Generation III	-11.4	1	
	Vein. Intermediate and final products of the Rayleigh fractionation of homogeneous fluid	+3.8 to +11.2	2	5.2

Standard deviation is based on individual spots